Journal of *Marine Science and Engineering*

MDPI

*Article*

# Multiobjective Optimization of the Performance and Emissions of a Large Low-Speed Dual-Fuel Marine Engine Based on MNLR-MOPSO

**Yujin Cong [1,*], Huibing Gan [1,*], Huaiyu Wang [2,*], Guotong Hu [1] and Yi Liu [1]**

[1] Marine Engineering College, Dalian Maritime University, Dalian 116026, China; huguotong@dlmu.edu.cn (G.H.); liu1120190109@dlmu.edu.cn (Y.L.)
[2] School of Mechanical Engineering, Beijing Institute of Technology, Beijing 100081, China
* Correspondence: 1120190082@dlmu.edu.cn (Y.C.); ghbzq@dlmu.edu.cn (H.G.); 3120205286@bit.edu.cn (H.W.)

**Abstract:** With increasingly strict emission regulations and growing environmental concerns, it is urgent to improve engine performance and reduce emissions. In this paper, multivariate nonlinear regression (MNLR) combined with multiobjective particle swarm optimization (MOPSO) was implemented to optimize the performance and emissions of a large low-speed two-stroke dual-fuel marine engine. First, a simulation model of a dual-fuel engine was established using AVL-BOOST software. Next, a single-factor scanning value method was applied to control a range of variables, including intake pressure, intake temperature, and natural gas mass fraction. Then, a nonlinear regression model was established using the statistical multivariate nonlinear regression equation. Finally, the multiobjective optimization algorithm implementing MOPSO was used to solve the trade-off between performance and emissions. It was found that when the intake pressure was 3.607 bar, the intake temperature was 297.15 K and the natural gas mass fraction was 0.962. The engine power increased by 0.34%, the brake specific fuel consumption (BSFC) reduced by 0.21%, and the NOx emissions reduced by 39.56%. The results show that the combination of multiple nonlinear regression and intelligent optimization algorithm is an effective method to optimize engine parameter settings.

**Keywords:** dual-fuel engine; performance and emission optimization; multiobjective particle swarm optimization; multivariate nonlinear regression

check for updates

**Citation:** Cong, Y.; Gan, H.; Wang, H.; Hu, G.; Liu, Y. Multiobjective Optimization of the Performance and Emissions of a Large Low-Speed Dual-Fuel Marine Engine Based on MNLR-MOPSO. *J. Mar. Sci. Eng.* **2021**, *9*, 1170. https://doi.org/10.3390/jmse9111170

Received: 18 September 2021
Accepted: 21 October 2021
Published: 25 October 2021

**Publisher's Note:** MDPI stays neutral with regard to jurisdictional claims in published maps and institutional affiliations.

**Copyright:** © 2021 by the authors. Licensee MDPI, Basel, Switzerland. This article is an open access article distributed under the terms and conditions of the Creative Commons Attribution (CC BY) license (https://creativecommons.org/licenses/by/4.0/).

## 1. Introduction

Large low-speed two-stroke diesel engines are widely used in marine application because of their advantages of higher efficiency, better economy, larger power range, and higher reliability [1]. In order to prevent pollution of the atmosphere and marine environment, the International Maritime Organization (IMO) has issued a series of laws and regulations. Compared to traditional fuels, natural gas has the characteristics of large reserves, high calorific value, and clean combustion and is considered to be one of the most developed alternative fuels [2]. Dual-fuel engines, which use alternative fuels such as natural gas as the main fuel, could be a solution to reduce emissions compared to traditional diesel engines [3]. In recent years, with the increasingly strict emission regulations and increasing shortage of petroleum energy, dual-fuel engines have attracted more and more attention. At present, research on dual-fuel engines has mainly focused on the performance of the new engine, combustion and emission characteristics, combustion model, lean-burn technology, pressurized intercooling technology, oil and gas electronic regulation and control, in-cylinder combustion technology to control emissions, out-of-machine catalytic technology, and exhaust gas recirculation technology [4].

Mavrelos and Theotokatos built a model of a large two-stroke dual-fuel marine engine to optimize the engine's overall performance by adjusting the parameters [5]. Stoupos et al. used GT-ISE software to study four-stroke marine engines and revealed the processes

that affect engine efficiency and gas emissions through analysis so as to explain in detail ways to improve engine efficiency and reduce emissions [6]. Abagnale and Cameretti used CFD software and experiments to discuss the effects of different fuel ratios on the performance and pollutant emissions of a natural gas and diesel common-rail diesel engine [7]. Zheng et al. used the 3D CFD software CONVERGE to study the effects of exhaust valve closing (EVC) time, exhaust gas recirculation (EGR), and pilot fuel injection time (PFIT) on generation of the harmful pollutant nitrogen oxide (NOx) in low-speed two-stroke dual-fuel marine engines [8]. Aldawood et al. used a single cylinder engine to conduct experiments under different loads, explored a method of controlling dual-fuel combustion in HCCI engine using multiobjective genetic algorithm, and proposed a comprehensive control strategy for natural gas/diesel engines [9]. Gonca and Sahin applied the steam injection method (SIM), miller cycle (MC), and turbocharging (TC) techniques to a four-stroke direct injection diesel engine. Experimental and numerical analysis showed that combination of the three techniques could minimize emissions from the diesel engine [10]. Zou et al. used MATLAB to build a two-zone combustion model of a four-stroke dual-fuel marine engine. Based on this model, they studied the effects of intake temperature, compression ratio, and natural gas intake on the knock of the dual-fuel engine [11]. Zhou et al. investigated the influence of miller cycle on knock and combustion characteristics of a single-cylinder gasoline engine, and the results showed that an appropriate miller cycle strategy could moderate engine knock [12]. Benajes et al. studied the influence of low-temperature combustion (LTC) on engine combustion by decreasing the intake oxygen concentration and advancing the intake valve closing angle. The results showed that the LTC strategy could reduce NOx and soot emissions but that fuel consumption would increase [13]. Belgiornoa and Dimitrakopoulos used a diesel engine to explore the influence of pilot quantity, combustion phasing, and EGR on the performance and emissions of gasoline partial premixed combustion. The results showed that partial premixed combustion and EGR could reduce soot and NOx emissions [14]. Ji et al. used the 3D CFD software CONVERGE to study the effects of miller cycle, EGR, intake air humidification, and fuel injection strategy on the performance of a low-speed two-stroke diesel engine. The results showed that EGR technology and intake humidification could greatly reduce NOx emissions [15]. Lee et al. used an optical diesel engine to study the effects of various natural gas substitution ratios on combustion and emissions. The results showed that under the condition of ensuring the same energy, a higher natural gas substitution rate resulted in cleaner combustion and better flame characteristics [16]. Khanjani et al. used response surface methodology (RSM) to study the effects of different formulations of emulsified fuel on engine performance and emissions, and the results showed that emulsified fuel could reduce engine emissions [17]. Şener and Gul optimized piston geometry using CONVERGE and CAESES software combined with multiobjective genetic algorithm (MOGA), and the results showed that the optimized piston could reduce NOx and soot emissions [18]. Golzari et al. studied the influence of water injection on the efficiency and emissions of a small single-cylinder gasoline direct injection engine, and the results showed that increasing water injection volume could improve the net efficiency of the engine while reducing emissions [19]. Stoumpos and Theotokatos used MOGA and design of experiment (DOE) parameters to optimize the engine and EGR/ABP (air bypass) system setting, and the results showed that the combination of EGR and ABP system enabled the engine emissions to meet more stringent regulatory requirements [20]. Cai et al. optimized the EGR rate using the multiobjective gray situation decision method and Pareto frontier analysis method. The research showed that the result of multiobjective gray situation decision was more inclined to EGR rate, while Pareto frontier analysis could obtain the solution with the minimum deviation from each optimization objective according to the bias degree of noninferior solution sensitivity ratio [21]. Wu and Wei used RSM to conduct multiparameter and multiobjective optimization research on the nonlinear phenomena existing between multiple parameters in the combustion system of direct injection diesel engine [22]. Kamarulzaman and Abdullah used RSM to optimize the performance and

emission parameters of a compression ignition engine. The results showed that at 92.72% load, the best performance was achieved at 6.43% *Hermetia illucens* larvae oil (HILO) and 93.57% diesel fuel mixture. The RSM optimization method has also been proven to be reliable for finding the optimal combination of engine performance and exhaust emission parameters [23]. Wang et al. established a large four-stroke dual-fuel marine engine model with AVL-BOOST and analyzed the effects of boost pressure, compression ratio, and the timing of intake valve closing on engine performance and emissions using this model. Then, RSM was used to optimize the emissions and performance to obtain the best parameters setting [24].

To sum up, engine performance and emission optimization has attracted the attention of a large number of researchers. However, most of the above references adopted one or multiple variable strategies to optimize engine performance and emissions, with few combining multivariable strategies with multiobjective optimization algorithms. Based on the briefly reviewed literature above, it can be concluded that the intake pressure, intake temperature, and natural gas mass fraction have a great influence on engine performance and emissions [25–27]. However, there have been few studies on engine performance and emission optimization that combine intake pressure, intake temperature, and natural gas mass fraction, especially in the field of large two-stroke dual-fuel marine engines. In order to make up for this research gap, this study applied the regression model and optimization algorithm to the performance and emission optimization of a large two-stroke dual-fuel marine engine and adopted multiparameter and multivariable simultaneous optimization strategy to explore the trade-off relationship between engine input parameters and performance and emissions. Because of the large size of marine engines, it is difficult to carry out corresponding experimental research. With the development of computer technology, numerical simulation has been widely accepted as the best way and partial alternative to study large marine engines because of its high efficiency and accuracy [28,29].

In this study, the engine simulation software AVL-BOOST was used to establish a simulation model of a large low-speed two-stroke dual-fuel marine engine and conduct model calibration. Three input parameters, namely intake pressure, intake temperature, and natural gas mass fraction, were selected to conduct simulation research. Then, the accuracy of the prediction model was verified by establishing a regression prediction model based on the simulation data using multiple nonlinear regression equation. Finally, MOPSO algorithm was used for multiobjective optimization, the main purpose of which was to obtain the best performance and the lowest emissions of the engine input parameter settings. The working routine of this paper is shown in Figure 1.

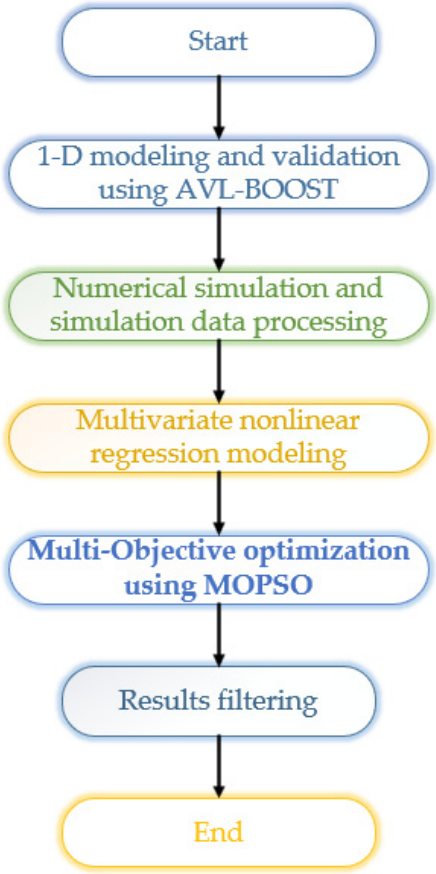



**Figure 1.** Summary of the working routine.

## 2. Modeling Methodology

### *2.1. Establishment and Calibration of the Simulation Model*

This study took MAN B&W 6S50ME-C-GI dual-fuel engine as the research object. The structure and principle of the dual-fuel engine are similar to the traditional diesel engine, but the fuel type is variable and the control system is complex. In gas mode, diesel oil is used as the ignition fuel to ignite natural gas, and the gas mode can be smoothly switched to diesel mode. The main parameters of the engine are shown in Table 1.

**Table 1.** Specification of the dual-fuel engine.

| Engine Parameters | Unit | Values |
|---|---|---|
| Cylinder number | - | 6 |
| Bore | mm | 500 |
| Stroke | mm | 2000 |
| Power | kW | 8100 |
| Speed | rpm | 108 |
| Fire order | - | 1-5-3-4-2-6 |

AVL-BOOST software was used to establish a model to study the performance and emissions of the dual-fuel engine. All measurement data for the engine are from [30,31] and shipyard bench test report.

As the Vibe heat release model is simple, practical, and widely used, it was used to calculate the heat release rate [32]. The model is described as follows:

$$\begin{cases} \frac{dx}{d\alpha} = \frac{\alpha}{\Delta\alpha_c} \cdot y^m \cdot e^{-a \cdot y(m+1)} \\ y = \frac{\alpha - \alpha_0}{\Delta\alpha_c} \end{cases} \quad (1)$$

The Woschni heat transfer model was adopted to calculate heat loss. This transforms the complicated heat transfer process into the heat transfer coefficient model, making the calculation simple and accurate [33]. The model is described as follows:

$$\alpha_w = C_0 D^{-0.2} p^{0.8} T^{-0.53} \times \left[ C_1 \cdot C_m + C_2 \cdot \frac{V_D T_1}{P_1 V_1} (p - p_{mot}) \right]^{0.8} \quad (2)$$

According to the test report and combined with the theoretical model, the engine in the AVL-BOOST environment was established as shown in Figure 2. The symbols of the main components in Figure 2 are explained in Table 2.

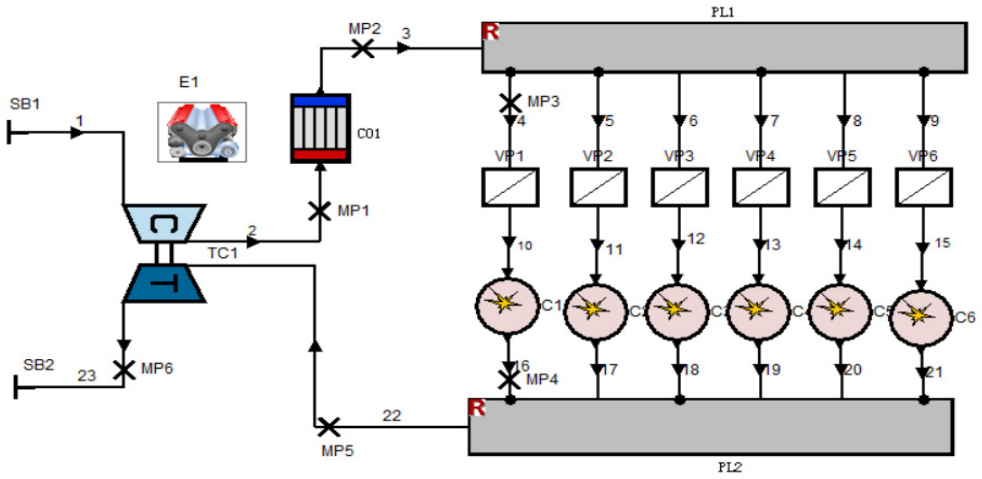



**Figure 2.** 6S50 ME-C-GI engine model in the AVL-BOOST environment.

**Table 2.** The main definitions of the symbols.

| NO. | Symbols | Element |
|---|---|---|
| 1 | SB1 | Intake boundary |
| 2 | SB2 | Exhaust boundary |
| 3 | E1 | Engine |
| 4 | TC1 | Turbocharger |
| 5 | CO1 | Cooler |
| 6 | MP1-6 | Measuring point |
| 7 | PL1 | Intake manifold |
| 8 | PL2 | Exhaust manifold |
| 9 | VP1-6 | Scavenge box |
| 10 | C1-6 | Cylinder |
| 11 | 1-23 | Pipe |

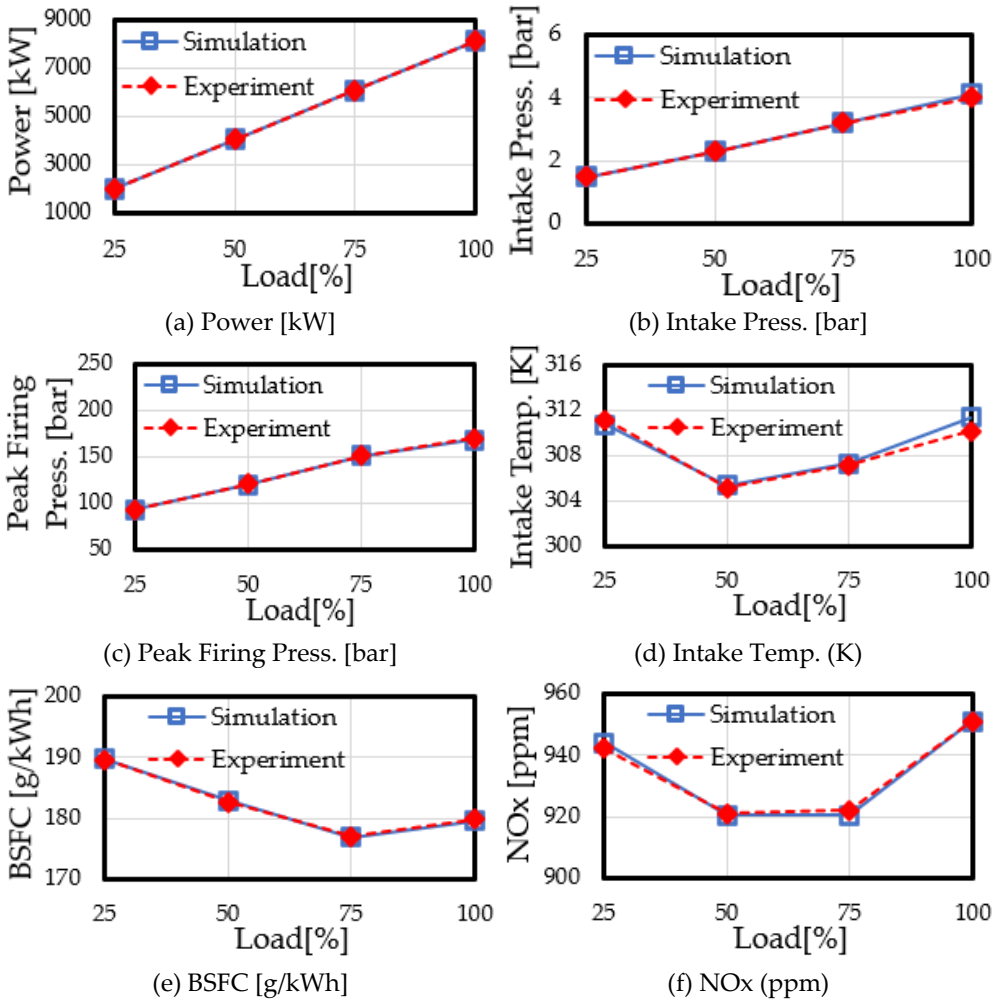
Because BOOST does not support simultaneous injection of two type fuels, a one-dimensional (1D) model in diesel mode was first established, followed by calibration and verification according to the method provided in [34,35]. First, the fuel injection setting in diesel mode was established. After verification, the fuel setting function in BOOST was used to set the fuel. On the premise of ensuring fuel injection quality, natural gas and diesel were mixed in proportion and treated as a single fuel.

Turbocharger (T/C) modeling has always been one of the difficulties in engine modeling. Because the aim was to study the engine intake and other parameter settings, for T/C, we did not establish the T/C model in detail but rather only used BOOST on its own, which is simple, practical, and widely accepted [24]. Because the ship engine studied here was not a constant-speed engine, the ship engine had different speeds under different loads according to the shipyard bench test report during modeling. Partial test data of the direct injection dual-fuel (DIDF) mode are shown in Table 3.

**Table 3.** Partial test data of the DIDF mode.

| NO. | | 1 | 2 | 3 | 4 |
|---|---|---|---|---|---|
| Load (%) | - | 25 | 50 | 75 | 100 |
| Speed (rpm) | - | 68 | 85.7 | 98.1 | 108 |
| Power (kW) | - | 2025 | 4050 | 6075 | 8100 |
| Exhaust | Cylinder out | 235 | 286 | 312 | 375 |
| Gas | Before T/C | 286 | 352 | 399 | 472 |
| Temperature (°C) | After T/C | 214 | 223 | 213 | 240 |
| T/C speed (rpm) | - | 8929 | 13,528 | 16,570 | 18,777 |
| Test room | Temperature (°C) | 26 | 25.6 | 25.7 | 25.1 |

Figure 3 shows a comparison between the simulation and experimental values of this dual-fuel engine in diesel mode, and Table 4 shows the errors of different loads in diesel mode. It can be seen from Figure 3 that the established 1D BOOST model ran accurately in diesel mode.




(a) Power [kW] (b) Intake Press. [bar]

(c) Peak Firing Press. [bar] (d) Intake Temp. (K)

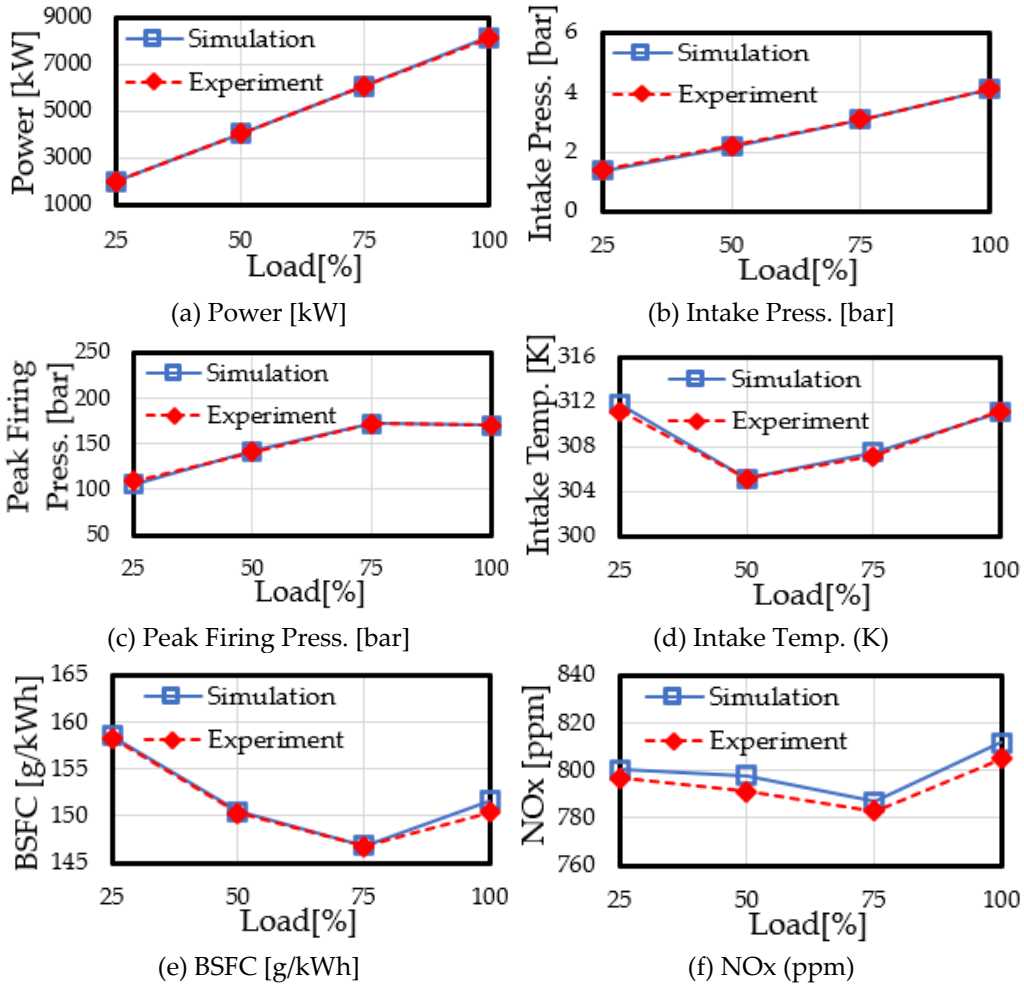
(e) BSFC [g/kWh] (f) NOx (ppm)

**Figure 3.** Validation results of primary parameter of the diesel mode.

**Table 4.** Calculation error of the diesel mode.

| Engine Load (%) | 100 | 75 | 50 | 25 |
|---|---|---|---|---|
| **Mode** | **Diesel Mode Error (%)** | | | |
| Power (kW) | 0.09 | −0.03 | −0.15 | −0.1 |
| Intake Pressure (bar) | 2.5 | 0 | −0.43 | 0 |
| Peak Firing Pressure (bar) | −1.3 | −0.57 | −0.28 | −0.77 |
| BSFC (g/kWh) | −0.09 | −0.1 | 0.14 | 0.07 |
| Intake Temperature (K) | 0.38 | 0.06 | 0.08 | −0.13 |
| NOx (ppm) | −0.02 | −0.15 | −0.07 | 0.2 |

Figure 4 shows a comparison between the simulation and experimental values of the dual-fuel engine in gas mode, and Table 5 shows the errors of different loads in gas mode. To sum up, as can be seen from the calculation in Tables 4 and 5, the errors between the simulation and experimental values of the main parameters of the model were within 3% in both diesel and gas modes, thus indicating the accuracy of the model and that it can be used for further research.




(a) Power [kW] (b) Intake Press. [bar]

(c) Peak Firing Press. [bar] (d) Intake Temp. (K)

(e) BSFC [g/kWh] (f) NOx (ppm)

**Figure 4.** Validation results of primary parameter of the gas mode.

**Table 5.** Calculation error of the gas mode.

| Engine Load (%) | 100 | 75 | 50 | 25 |
|---|---|---|---|---|
| Mode | Gas Mode Error (%) | | | |
| Power (kW) | 0.36 | −0.06 | −0.14 | 0.1 |
| Intake Pressure (bar) | 0 | 0 | −0.9 | −0.71 |
| Peak Firing Pressure (bar) | 0.17 | −0.05 | 0.13 | −2.83 |
| BSFC (g/kWh) | 0.8 | 0.08 | 0.14 | 0.17 |
| Intake Temperature (K) | −0.02 | 0.11 | 0.01 | 0.21 |
| NOx (ppm) | 0.83 | 0.5 | 0.88 | 0.42 |

Considering the large NOx emissions under 75% load, which is the most commonly used load in ships and the load with the largest weight in the ship ISO8178E3 test cycle, accounting for about 50% [36], we optimized the emissions and performance of the dual-fuel engine under 75% load. Table 6 shows the performance and emission simulation data of the dual-fuel engine with different intake pressures (2.5–3.7 bar), intake temperatures (297.15–327.15 K), and natural gas mass fractions (6.2–96.2%).

**Table 6.** The simulation data of DF engine.

| NO. | Intake Pressure (bar) ($x_1$) | Intake Temperature (K) ($x_2$) | Natural Gas Mass Fraction ($x_3$) | Power (kW) ($y_1$) | BSFC (g/kWh) ($y_2$) | NOx (ppm) ($y_3$) | Peak Firing Pressure (bar) ($y_4$) |
|---|---|---|---|---|---|---|---|
| 1 | 2.5 | 297.15 | 0.962 | 5979.29 | 149.09 | 1135.26 | 152.42 |
| 2 | 2.7 | 297.15 | 0.962 | 6032.21 | 147.78 | 938.87 | 159.26 |
| 3 | 2.9 | 297.15 | 0.962 | 6082.17 | 146.57 | 793.10 | 166.51 |
| 4 | 3.1 | 297.15 | 0.962 | 6128.70 | 145.45 | 686.18 | 173.85 |
| 5 | 3.3 | 297.15 | 0.962 | 6151.23 | 144.92 | 608.36 | 180.77 |
| 6 | 3.5 | 297.15 | 0.962 | 6111.25 | 145.87 | 533.98 | 186.21 |
| 7 | 3.7 | 297.15 | 0.962 | 6064.91 | 146.98 | 459.65 | 191.50 |
| 8 | 2.5 | 307.15 | 0.962 | 5926.61 | 150.41 | 1332.67 | 151.18 |
| 9 | 2.7 | 307.15 | 0.962 | 5979.05 | 149.09 | 1103.79 | 157.96 |
| ⋮ | ⋮ | ⋮ | ⋮ | ⋮ | ⋮ | ⋮ | ⋮ |
| 109 | 3.1 | 327.15 | 0.062 | 5155.28 | 172.92 | 786.25 | 161.25 |
| 110 | 3.3 | 327.15 | 0.062 | 5142.20 | 173.36 | 701.28 | 167.36 |
| 111 | 3.5 | 327.15 | 0.062 | 5096.41 | 174.92 | 611.44 | 172.54 |
| 112 | 3.7 | 327.15 | 0.062 | 5049.04 | 176.56 | 514.79 | 177.47 |

### *2.2. Establishment of Multivariate Nonlinear Regression Model Based on SPSS*

SPSS is one of the most popular statistical analysis software. It is widely used in economy, biology, education, health, scientific research, sports, business and finance, and many other fields [37].

Multivariate nonlinear regression analysis is used to model the nonlinear relationship between multiple independent variables and dependent variables, and one of the commonly used methods is curve fitting, which is establishes the mathematical relationships between given discrete data points [38]. The multivariate nonlinear regression model adopted in this study can be described as follows:

$$y_i = a + b \cdot x_1 + c \cdot x_2 + d \cdot x_3 + e \cdot x_1^2 + f \cdot x_2^2 + g \cdot x_3^2 + h \cdot x_1 \cdot x_2 + i \cdot x_2 \cdot x_3 + j \cdot x_1 \cdot x_3 \quad (3)$$

where $y_i$ is the dependent variables, including power, brake specific fuel consumption (BSFC), NOx emissions, and peak firing pressure (PFP); $x_1$ , $x_2$ , and $x_3$ represent the intake pressure, intake temperature, and natural gas mass fraction, respectively; $a$ represents the constant term; $b$, $c$, and $d$ represent the regression coefficients of the primary term; $e$ , $f$, and $g$ represent the quadratic term coefficients; and $h$ , $i$ , and $j$ represent the cross-term coefficients.

The multivariate nonlinear regression model was established according to the samples, and all fitting coefficients were reserved to six decimal places. Here, power regression was used as an example, and the nonlinear regression results are shown in Table 7.

**Table 7.** Parameter estimates.

| Parameter | Estimation | Standard Error | 95% Confidence Interval | |
|---|---|---|---|---|
| | | | Lower Limit | Upper Limit |
| $a$ | 6431.583340 | 1336.381482 | 3780.877006 | 9082.289673 |
| $b$ | 817.122254 | 110.896242 | 597.160083 | 1037.084425 |
| $c$ | −13.120762 | 8.391915 | −29.766086 | 3.524562 |
| $d$ | 900.792557 | 116.437965 | 669.838406 | 1131.746708 |
| $e$ | −269.509686 | 9.638417 | −288.627441 | −250.391931 |
| $f$ | 0.003198 | 0.013356 | −0.023293 | 0.029688 |
| $g$ | −22.074143 | 14.839339 | −51.507900 | 7.359615 |
| $h$ | 2.624122 | 0.298635 | 2.031780 | 3.216464 |
| $i$ | −1.379366 | 0.356143 | −2.085773 | −0.672958 |
| $j$ | 165.728262 | 9.954509 | 145.983540 | 185.472985 |

The estimated regression values of each coefficient were obtained from Table 7, and the estimated regression values of the coefficients in Table 7 were substituted into Equation (3). The power regression model obtained was as follows:

$$y_1 = 6431.583340 + 817.122254x_1 - 13.120762x_2 + 900.792557x_3 - 269.509686x_1^2 + 0.003198x_2^2 - 22.074143x_3^2 + 2.624122x_1x_2 - 1.379366x_2x_3 + 165.728262x_1x_3 \quad (4)$$

Similarly, the regression model of BSFC can be written:

$$y_2 = 139.577779 - 22.850600x_1 + 0.333743x_2 - 20.822960x_3 + 7.949033x_1^2 + 0.000040x_2^2 + 5.318451x_3^2 - 0.081929x_1x_2 + 0.003033x_2x_3 - 4.274703x_1x_3 \quad (5)$$

The regression model of NOx emission is:

$$y_3 = -985.739375 + 4.134159x_1 + 3.639901x_2 - 301.840475x_3 + 304.650315x_1^2 + 0.049343x_2^2 - 8.488980x_3^2 - 7.571306x_1x_2 + 4.243117x_2x_3 - 217.682576x_1x_3 \quad (6)$$

The regression model of the PFP is:

$$y_4 = 100.053303 + 50.000641x_1 - 0.319463x_2 + 10.751954x_3 - 5.468750x_1^2 + 0.000138x_2^2 - 0.156754x_3^2 + 0.046875x_1x_2 - 0.028971x_2x_3 + 3.018452x_1x_3 \quad (7)$$

### 2.3. Multiobjective Optimization Method

Most engineering problems have a multiobjective formula, and trade-offs often occur between the parameters. It is not possible to achieve a single solution that optimizes all objectives simultaneously. Therefore, the Pareto frontier alternative is the best choice in practice [39,40]. Particle swarm optimization (PSO) algorithm can be divided into single-objective and multiobjective particle swarm optimization. Usually, multiobjective problems can be transformed into single-objective problems by weighting, but the weight has a great influence on the optimization results. For engine multiobjective optimization, multiple objectives need to be optimized simultaneously. MOPSO has become the main research direction of multiobjective optimization due to its advantages of high efficiency and speed [41]. This takes power, NOx emissions, and BSFC as research objects. Its purpose is to obtain higher power, lower NOx emissions, and lower BSFC at the same time, as shown in Equation (8):

$$\begin{cases} maxy_1(\text{Power}) \\ miny_2(\text{BSFC}) \\ miny_3(\text{NOx}) \end{cases} \quad (8)$$

For the maximum problem, we usually take the opposite direction of the target value; when the optimal solution is obtained, the opposite direction is taken. The population size of MOPSO adopted in this study was 100, and the maximum number of iterations was 100. In order to better control the search ability of the algorithm, MOPSO algorithm with weights was adopted [42]. Particle motion calculation in iteration $(t + 1)$ is shown in Equation (9):

$$\begin{cases} x_i(t+1) = x_i(t) + v_i(t+1) \\ v_i(t+1) = \omega \cdot v_i(t) + c_1 r_1 \cdot (pbest_i(t) - x_i(t)) + c_2 r_2 (gbest(t) - x_i(t)) \end{cases} \quad (9)$$

where $i = 1, 2, 3 \ldots n$ —represents the indexed particle; $x_i(t)$ represents the position of the $i$-th particle at the $i$-th iteration; $v_i(t)$ represents the velocity of the $i$-th particle at the $i$-th iteration; $gbest(t)$ is the global optimal position; and $pbest_i(t)$ is the individual optimal position found so far for the $i$-th particle; $\omega$ is the inertia weight of the current particle; $c_1$ , $c_2$ are acceleration factors; and $r_1$ , $r_2$ are random values uniformly distributed in the interval [0,1].

Experiments have shown that when the weight factor is 0.7298 and the acceleration factor is 1.49618, the convergence of the algorithm is good [43,44]. Therefore, the weight factor of 0.7298 and the acceleration factor of 1.49618 was used in this study. The specific optimization process is shown in Figure 5.

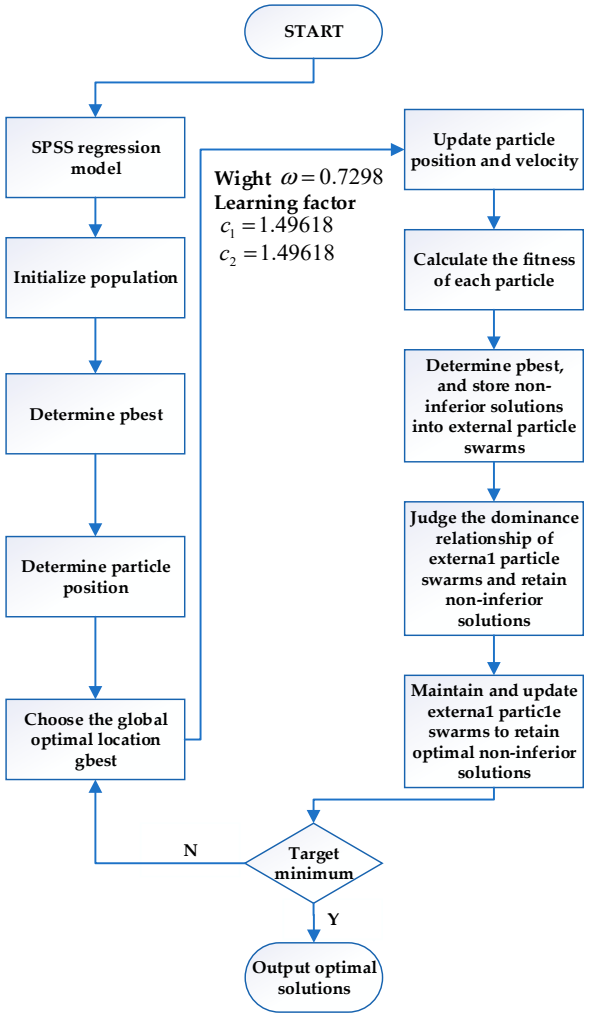



**Figure 5.** Flowchart of the MOPSO algorithm.

## 3. Results and Discussion

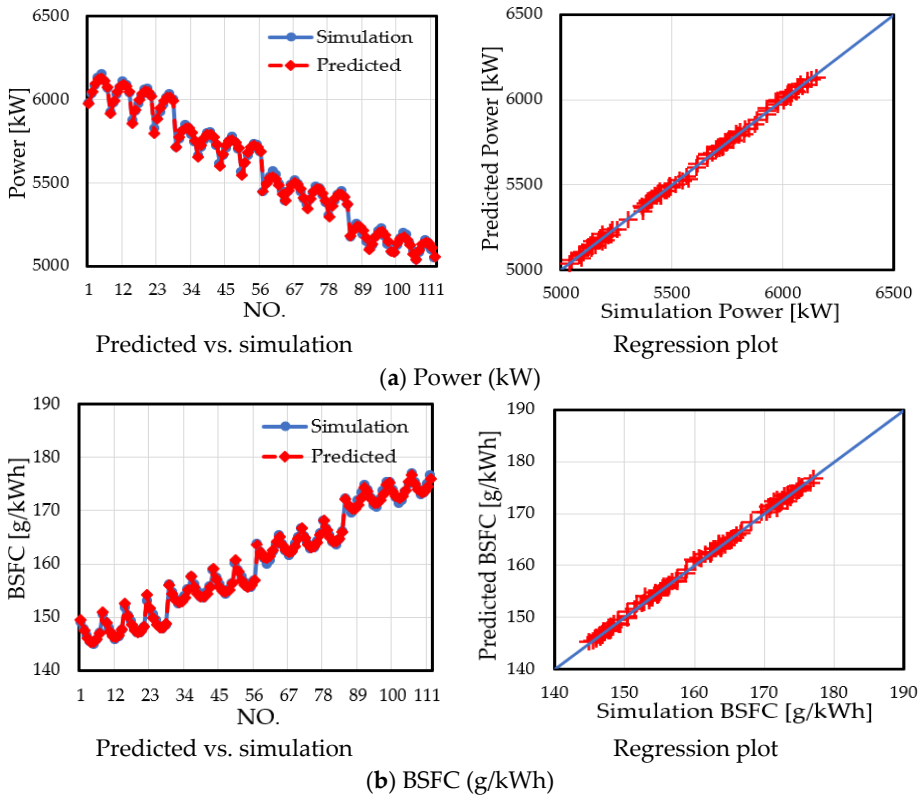
### 3.1. Regression Analysis

Table 8 shows the variance analysis of multivariate nonlinear return equation of power, from which $R^2 = 0.998$ could be obtained. In the same way, the regression equations $R^2$ of BSFC, NOx emissions, and PFP analyzed by SPSS software were 0.998, 0.992, and 0.999, respectively. As $R^2$ was greater than 0.98, indicating a high prediction ability, it can be further used in this investigation [45,46].

**Table 8.** Analysis of variance table.

| Source | Quadratic Sum | Degree of Freedom | Mean Square |
|---|---|---|---|
| Regression | 3,502,751,999.441904 | 10.000000 | 350,275,199.944190 |
| Residual | 20,376.532796 | 102.000000 | 199.769929 |
| Uncorrected total | 3,502,772,375.974700 | 112.000000 | - |
| Corrected total | 12,132,592.385299 | 111.000000 | - |
| Dependent variable: $y_1$ | | | |
| a $R^2$ = 1 − (Sum of squares of residuals)/(Correct the sum of squares) = 0.998. | | | |

Figure 6 shows a comparison of the predicted and simulated values for power, BSFC, NOx emissions, and PFP with simulation data. By comparing the predicted and simulated values, the established multivariate nonlinear regression equation could well predict engine performance and emissions. From the regression curve, the predicted value was close to the actual value, indicating that the multivariate nonlinear equation could estimate the performance and emissions simultaneously with excellent accuracy for predicting the small sample regression problem of dual-fuel engine performance and emissions [47].




Predicted vs. simulation | Regression plot

(**a**) Power (kW)

Predicted vs. simulation | Regression plot

(**b**) BSFC (g/kWh)

**Figure 6.** *Cont.*

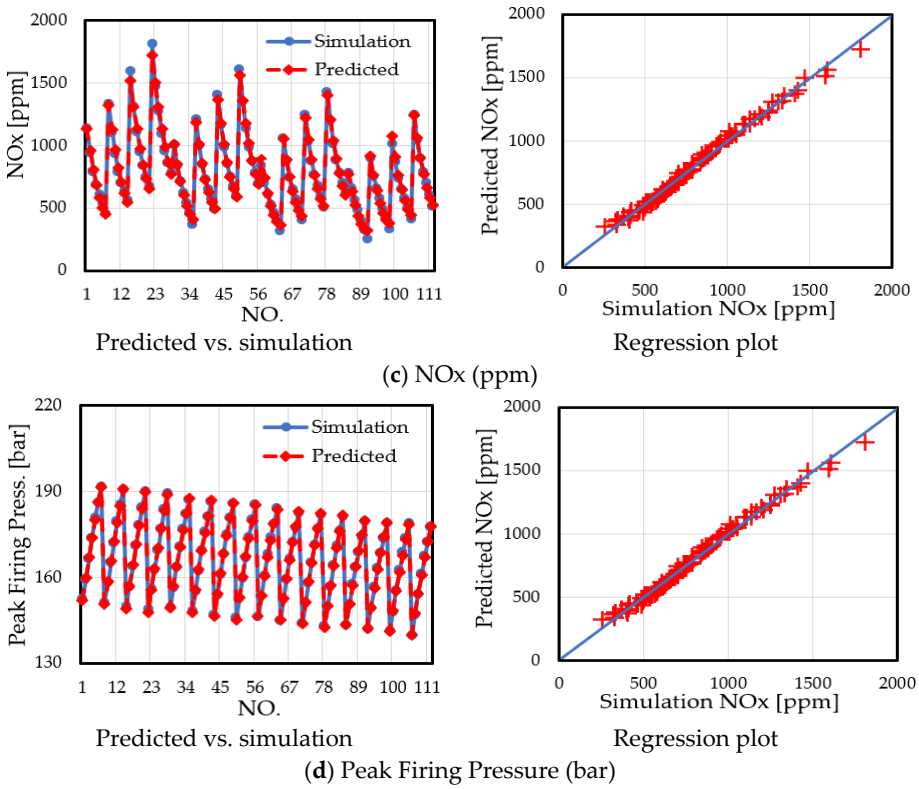
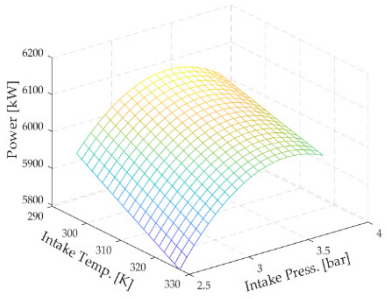



**Figure 6.** Comparison of predicted vs. simulation values.

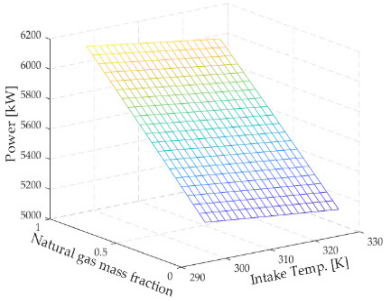
### *3.2. Operating Parameter Analysis*

Based on the regression equation, the response surfaces of the power, BSFC, NOx emissions, and PFP were established.

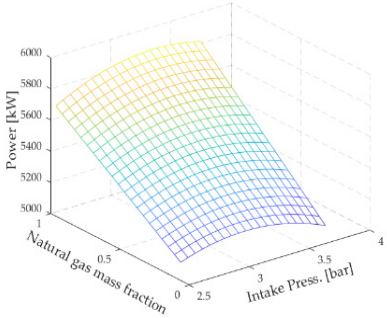
As can be seen from Figure 7, with the increase in intake pressure, the power of the dual-fuel engine first increased and then decreased, while the BSFC first decreased and then increased. This occurred because appropriate increase in intake pressure led to the increase in oxygen content in each cycle into the cylinder. The total amount of air increased, so the turbulent kinetic energy of the mixed gas in the cylinder increased. The oil and air mixture was more uniform, and the combustion was more sufficient, which was conducive to improving the performance of the engine. With the increase in intake pressure, the NOx emissions of the dual-fuel engine decreased gradually, while the PFP increased gradually. This was because the increase in intake pressure increased the average pressure in the cylinder, resulting in higher peak firing pressure. At the same time, the increase in intake pressure led to the increase in air intake. The hot melting of the working medium was larger, and the temperature in the fuel heat release cylinder was reduced, which reduced the temperature of nitrogen staying in the high temperature oxygen-rich environment, thus inhibiting generation of NOx [48].




Natural gas mass fraction = 0.962

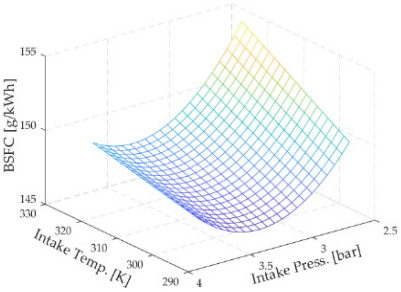



Intake pressure = 3.1 bar

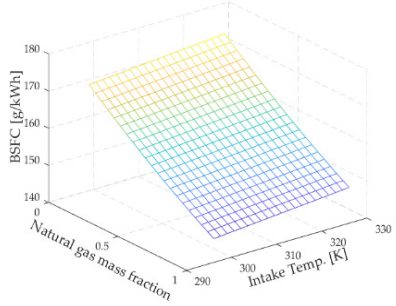



Intake temperature = 307.15 K

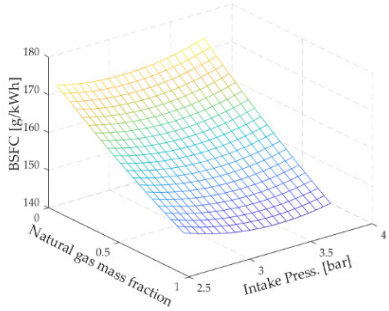
(**a**) Power (kW)




Natural gas mass fraction = 0.962



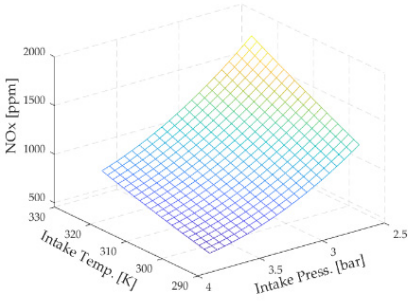

Intake pressure = 3.1 bar



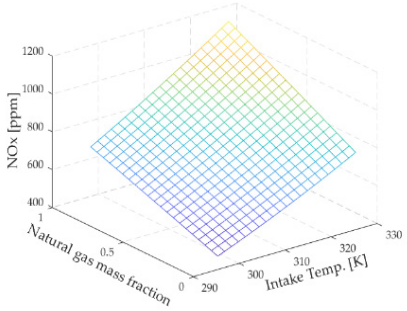

Intake temperature = 307.15 K

(**b**) BSFC (g/kWh)

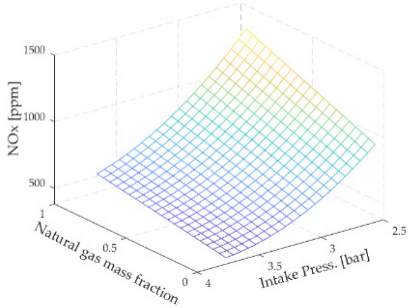
**Figure 7.** *Cont*.




Natural gas mass fraction = 0.962

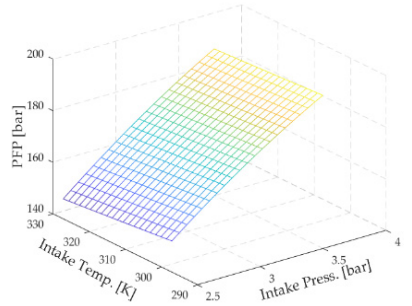



Intake pressure = 3.1 bar

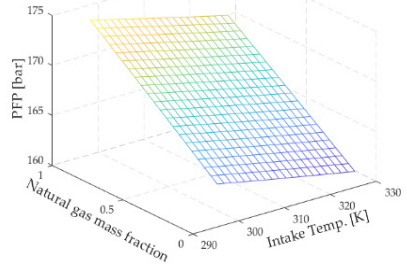



Intake temperature = 307.15 K

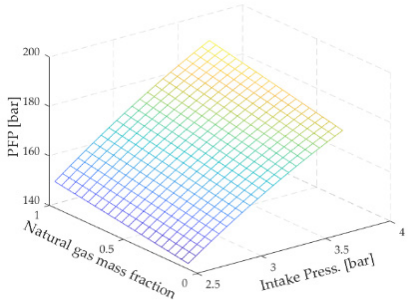
(**c**) NOx (ppm)




Natural gas mass fraction = 0.962




Intake pressure = 3.1 bar




Intake temperature = 307.15 K

(**d**) Peak Firing Pressure (bar)

**Figure 7.** The surface of the different responses.

As can be seen from Figure 7, with the increase in natural gas mass fraction, the power of the dual-fuel engine gradually increased, and the PFP and NOx emissions during combustion also gradually increased. However, with the increase in natural gas mass fraction, the BSFC of the dual-fuel engine gradually decreased. This was due to the increase in the natural gas mass fraction. The low calorific value of natural gas is higher than that

of diesel oil under the same quality guarantee conditions, and the heat release of natural gas is higher than that of diesel oil. This caused the average pressure in the cylinder to increase when the combustion heat was released, resulting in the increase in PFP of combustion. Due to the increase in heat release, the average temperature in the cylinder increased. The increase in natural gas mass fraction led to the increase in average pressure and average temperature in the cylinder, which was conducive to the high temperature and high pressure environment of NOx generation.

As can be seen from Figure 7, with the increase in intake temperature, the power and PFP of the dual-fuel engine gradually decreased, and the BSFC and NOx emissions gradually increased. This was because the increase in the intake temperature led to an increase in the initial temperature in the cylinder, which increased the average temperature of the combustion process, making the fuel injected into the cylinder more likely to ignite and providing a favorable high temperature environment for the formation of NOx.

To sum up, reasonable intake pressure is beneficial to improve the overall performance of dual-fuel engines, while higher intake pressure will reduce the engine power and improve the BSFC of the engine. However, for NOx emissions, higher intake pressure reduces NOx emissions and reduces environmental pollution. The reduction in intake temperature and improvement of natural gas mass fraction are conducive to improving the engine performance and reducing NOx emissions. Therefore, under the premise of meeting the actual situation, it is very important to obtain reasonable intake pressure, intake temperature. and natural gas mass fraction for improving engine performance and reducing NOx emission.

### 3.3. MOPSO Optimization Results

This study aimed to achieve the highest power, lowest BSFC, and lowest NOx emissions. Therefore, the previously established regression model was used as the proxy model of the dual-fuel engine, taking power, BSFC, and NOx emissions as targets, combined with MOPSO algorithm optimization. The overall distribution of the optimized multiobjective is shown in Figure 8. It should be noted that negative power in the figure does not mean the power is negative; this symbol is just a way for MOPSO to calculate the minimum value. Because maximum power is required, we usually convert the maximum value problem to the minimum value problem and then calculate the reverse [49].

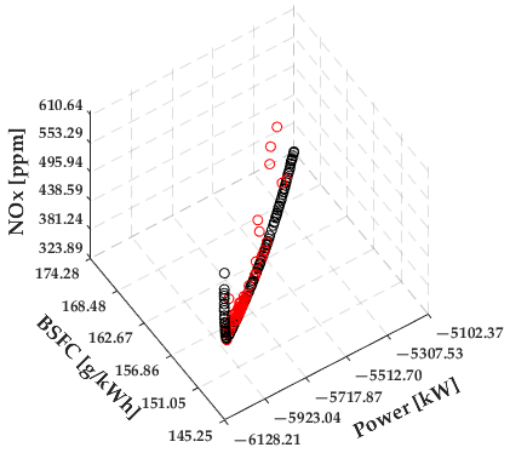
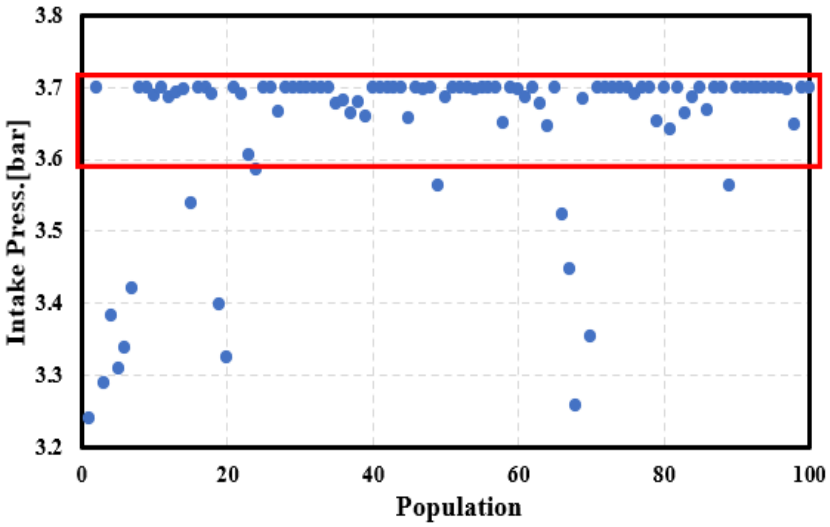
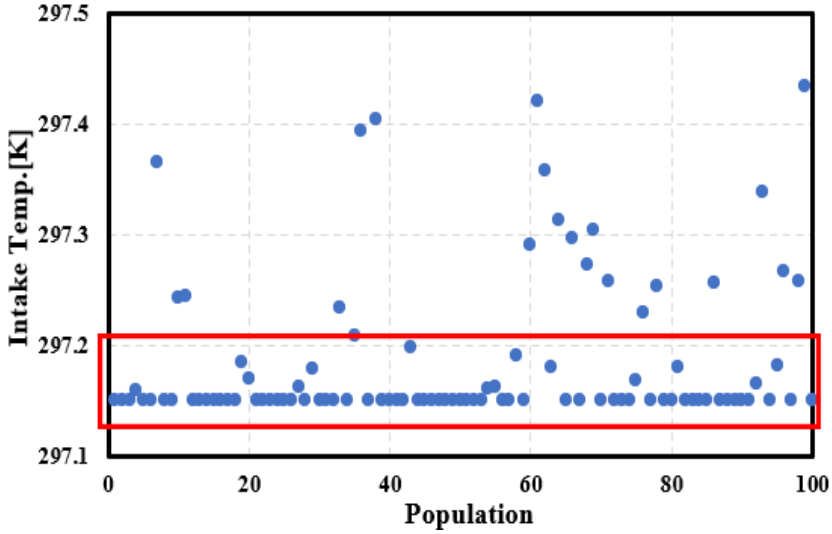



**Figure 8.** Overall distribution of goals.

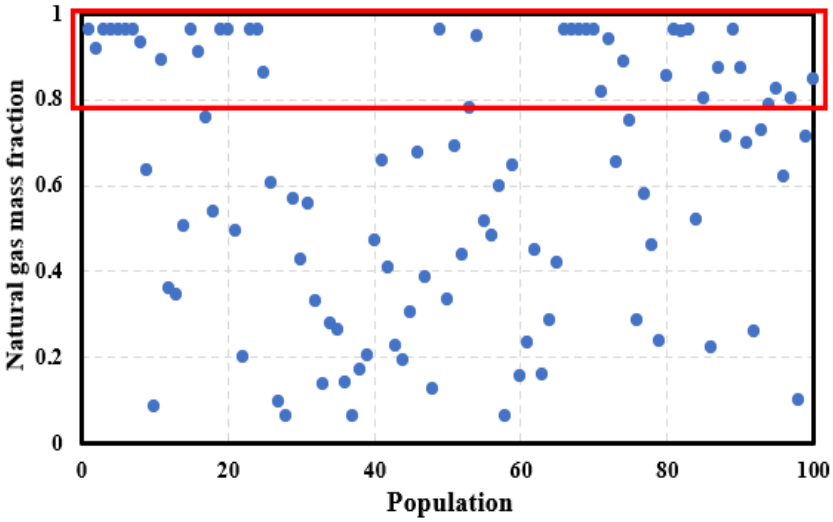
Figure 9 shows the overall distribution of the optimal solution after MOPSO optimization. As can be seen from the box area in Figure 9a, the optimal value range of the intake pressure was 3.6–3.7 bar. From the box area in Figure 9b, the optimal value range of the intake temperature was 297.15–297.20 K, and from the box area in Figure 9c, the optimal value range of the natural gas mass fraction was 0.8–0.962. On this basis, the optimal solution was selected.




(**a**) Solution set of intake pressure




(**b**) Solution set of intake temperature




(**c**) Solution set of natural gas mass fraction

**Figure 9.** Population distribution in the optimal solutions.

For the dual-fuel marine engine studied in this work, power as high power as possible and BSFC and NOx emissions as low as possible was required. By selecting power greater than or equal to 6000 kW and NOx emissions less than or equal to 480 ppm, the filtered optimal solutions are illustrated in Table 9. As can be seen from the box selection in Table 9, the value range of the optimal solution was consistent. On this basis, taking the lower BSFC as the target, the intake pressure was 3.607 bar, the intake temperature was 297.15 K, and the natural gas mass fraction was 0.962. The corresponding dual-fuel engine had a power of 6095.583 kW, BSFC of 146.389 g/kWh, and NOx emissions of 475.658 ppm. Compared with the values before optimization, the power increased by 0.34%, BSFC reduced by 0.21%, and NOx emissions reduced by 39.56%. Therefore, the optimization results obtained by MOPSO were very satisfactory in terms of reducing NOx emissions and improving power performance and fuel economy.

**Table 9.** Optimal solutions for satisfying constraints.

| Intake Pressure (bar) | Intake Temperature (K) | Natural Gas Mass Fraction | Power (kW) | BSFC (g/kWh) | NOx (ppm) |
|---|---|---|---|---|---|
| 3.700 | 297.245 | 0.893 | 6001.997 | 148.814 | 445.591 |
| 3.700 | 297.150 | 0.909 | 6018.877 | 148.400 | 446.920 |
| 3.700 | 297.150 | 0.919 | 6030.272 | 148.122 | 448.399 |
| 3.700 | 297.150 | 0.933 | 6044.708 | 147.770 | 450.271 |
| 3.700 | 297.150 | 0.939 | 6051.243 | 147.612 | 451.118 |
| 3.698 | 297.161 | 0.949 | 6062.025 | 147.347 | 452.994 |
| 3.700 | 297.150 | 0.960 | 6073.935 | 147.064 | 454.054 |
| 3.685 | 297.305 | 0.962 | 6078.820 | 146.918 | 458.815 |
| 3.663 | 297.150 | 0.962 | 6084.079 | 146.756 | 462.045 |
| 3.641 | 297.181 | 0.962 | 6088.657 | 146.610 | 467.393 |
| 3.607 | 297.150 | 0.962 | 6095.583 | 146.389 | 475.658 |

## 4. Conclusions

In this study, based on the MNLR-MOPSO method, the operation parameters of a large low-speed dual-fuel marine engine was optimized. The effect of operational parameter setting on the performance, combustion, and emissions was further studied based on the MNLR model. The main conclusions of this study can be drawn as follows:

- A 1D simulation model established through AVL-BOOST software was developed and validated based on experimental investigation for dual-fuel engine optimization. The pure diesel mode model was first established and then modified into natural gas–diesel dual-fuel mode. The maximum error was 2.5% for the diesel mode and 2.83% for the dual-fuel mode. The trend of the simulation model was consistent with the experimental data, which is suitable for the prediction of performance, combustion, and emission under various working conditions.
- The multivariate nonlinear regression (MNLR) model was implemented using SPSS software, and 112 samples were provided by the 1D simulation model. The $R^2$ of the power, BSFC, NOx emissions, and PFP was greater than 0.98, indicating the accuracy of the regression model and that it can be used for further studies.
- Through analysis of the regression prediction model, it was found that with the increase in intake pressure, the power of the dual-fuel engine increased first and then decreased, while BSFC decreased first and then increased, NOx emissions gradually decreased, and PFP gradually increased. With the increase in intake temperature, the power and PFP of dual-fuel engine gradually decreased, while BSFC and NOx emissions gradually increased. Under the condition of guaranteed fuel injection quality, with the increase in natural gas mass fraction, the power and PFP of the dual-fuel engine gradually increased. The NOx emissions also gradually increased, but the BSFC gradually decreased.

- According to the trade-off relationship between various objectives and parameters of the dual-fuel engine, the regression model was used as a proxy model and the MOPSO optimization algorithm was used to optimize the solution. The optimal value range of the intake pressure, intake temperature, and natural gas mass fraction was optimized, and the optimal value range of intake pressure was 3.6–3.7 bar. The optimal value range of intake temperature was 297.15–297.25 K, and the optimal value range of natural gas mass fraction was 0.8–0.962. On this basis, with high power, low BSFC, and low NOx emissions as the target, the optimal intake pressure was 3.607 bar, the intake temperature was 297.15 K, the natural gas mass fraction was 0.962, the power obtained was 6095.583 kW, and BSFC was 146.389 g/kWh. NOx emissions were 475.658 ppm. Compared with the values before optimization, the power of the dual-fuel engine increased by 0.34%, the BSFC reduced by 0.21%, and the NOx emissions reduced by 39.56%.

In conclusion, the present study provides an approach to modeling and optimizing large low-speed dual-fuel marine engines. The results contribute to a better understanding of the effects of operating parameters on performance and emissions. In this study, the multiple nonlinear regression equation of statistics was applied to predict performance and emissions of a dual-fuel engine, and the MOPSO optimization algorithm was combined to work out the engine parameter settings under the condition of satisfying performance and emission targets. When the intake pressure was 3.607 bar, the intake temperature was 297.15 K, and the natural gas replacement rate was 0.962. The power obtained increased by 0.34%, while the fuel consumption and NOx emissions reduced by 0.21% and 39.56%, respectively.

In future work, we will optimize the operating parameters of the dual-fuel engine at full load and apply the combination of machine learning and optimization algorithm to the prediction model of a dual-fuel engine.

**Author Contributions:** Author Contributions: Conceptualization, Y.C. and H.W.; methodology, Y.C.; software, Y.C.; validation, Y.C., H.G., and H.W.; formal analysis, H.G.; investigation, Y.C., G.H., and Y.L.; resources, H.G.; data curation, H.W., G.H.; writing—original draft preparation, Y.C.; writing—review and editing, H.G. and H.W.; visualization, H.G.; supervision, H.G.; project administration, H.G.; funding acquisition, H.G. All authors have read and agreed to the published version of the manuscript.

**Funding:** The research work has been financially supported by the People's Republic of China Project "Intelligent Ship Comprehensive Testing and Verification Research" ([2018] NO.473) as well as "the Fundamental Research Funds for the Central Universities" (NO.3132019315).

**Institutional Review Board Statement:** Not applicable.

**Informed Consent Statement:** Not applicable.

**Data Availability Statement:** The data used to support the findings of this study are available from the corresponding author upon request.

**Acknowledgments:** The authors also gratefully acknowledge the helpful comments and suggestions of the reviewers, which have improved the presentation of this paper.

**Conflicts of Interest:** The authors declare no conflict of interest.

## References

1. Zhu, L.; Li, B.; Li, A.; Ji, W.; Qian, Y.; Lu, X.; Huang, Z. Effects of fuel reforming on large-bore low-speed two-stroke dual fuel marine engine combined with EGR and injection strategy. *Int. J. Hydrogen Energy* **2020**, *45*, 29505–29517. [CrossRef]
2. George, D.G.; Eleftherios, K.D.; Chariklia, G.A.; George, D.G.; Eleftherios, K.D.; Chariklia, G.A. LNG carrier two-stroke propulsion systems: A comparative study of state of the art reliquefaction technologies. *Energy* **2020**, *195*, 116997. [CrossRef]
3. Yu, H.; Duan, S.; Sun, P. Comparative analysis between natural gas/diesel (dual fuel) and pure diesel on the marine diesel engine. *J. Eng. Res.* **2015**, *3*. [CrossRef]
4. Li, Y.; Wang, Q. Research Status of Natural Gas/Diesel Dual Fuel Engine. *Chem. Eng. Des. Commun.* **2016**, *42*, 87–88.

5. Mavrelos, C.; Theotokatos, G. Numerical investigation of a premixed combustion large marine two-stroke dual fuel engine for optimising engine settings via parametric runs. *Energy Convers. Manag.* **2018**, *160*, 48–59. [CrossRef]
6. Stoumpos, S.; Theotokatos, G.; Boulougouris, E.; Vassalos, D.; Lazakis, I.; Livanos, G. Marine dual fuel engine modelling and parametric investigation of engine settings effect on performance-emissions trade-offs. *Ocean Eng.* **2018**, *157*, 376–386. [CrossRef]
7. Abagnale, C.; Cameretti, M.C.; De Simio, L.; Gambino, M.; Iannaccone, S.; Tuccillo, R. Numerical Simulation and Experimental Test of Dual Fuel Operated Diesel Engines. *Appl. Therm. Eng.* **2014**, *65*, 403–417. [CrossRef]
8. Zheng, Z.; Li, C.; Ye, Y.; Liu, T.; Liu, B.; Wu, Z.; Dong, J.; Liu, H.; Yao, M. Numerical Simulation of Clean Combustion Strategy for Low-Pressure Injection Natural Gas Dual-Fuel Marine Engine. *J. Combust. Sci. Technol.* **2020**, *26*, 212–218.
9. Aldawood, A.; Mosbach, S.; Kraft, M. *HCCI Combustion Control Using Dual-Fuel Approach: Experimental and Modeling Investigations*; SAE: New York, NY, USA, 2012.
10. Gonca, G.; Sahin, B. Effect of turbo charging and steam injection methods on the performance of a Miller cycle diesel engine (MCDE). *Appl. Therm. Eng.* **2017**, *118*, 138–146. [CrossRef]
11. Zou, F.-K.; Zeng, H.; Wang, H.-Y.; Wang, X.-X.; Xu, Z.-X. Implementation and Parameter Analysis of the Knock Phenomenon of a Marine Dual-Fuel Engine Based on a Two-Zone Combustion Model. *Processes* **2021**, *9*, 602. [CrossRef]
12. Zhou, L.; Song, Y.; Hua, J.; Liu, F.; Wei, H. Effects of miller cycle strategies on combustion characteristics and knock resistance in a spark assisted compression ignition (SACI) engine. *Energy* **2020**, *206*, 118119. [CrossRef]
13. Benajes, J.; Molina, S.; Novella, R.; Belarte, E. Evaluation of massive exhaust gas recirculation and Miller cycle strategies for mixing-controlled low temperature combustion in a heavy duty diesel engine. *Energy* **2014**, *71*, 355–366. [CrossRef]
14. Belgiorno, G.; Dimitrakopoulos, N.; Di Blasio, G.; Beatrice, C.; Tunestål, P.; Tunér, M. Effect of the engine calibration parameters on gasoline partially premixed combustion performance and emissions compared to conventional diesel combustion in a light-duty Euro 6 engine. *Appl. Energy* **2018**, *228*, 2221–2234. [CrossRef]
15. Ji, W.; Li, A.; Lu, X.; Huang, Z.; Zhu, L. Numerical study on NOx and ISFC co-optimization for a low-speed two-stroke engine via Miller cycle, EGR, intake air humidification, and injection strategy implementation. *Appl. Therm. Eng.* **2019**, *153*, 398–408. [CrossRef]
16. Lee, C.-F.; Pang, Y.; Wu, H.; Nithyanandan, K.; Liu, F. An optical investigation of substitution rates on natural gas/diesel dual-fuel combustion in a diesel engine. *Appl. Energy* **2020**, *261*, 114455. [CrossRef]
17. Khanjani, A.; Sobati, M.A. Performance and emission of a diesel engine using different water/waste fish oil (WFO) biodiesel/diesel emulsion fuels: Optimization of fuel formulation via response surface methodology (RSM). *Fuel* **2021**, *288*, 119662. [CrossRef]
18. Şener, R.; Gül, M.Z. Optimization of the combustion chamber geometry and injection parameters on a light-duty diesel engine for emission minimization using multi-objective genetic algorithm. *Fuel* **2021**, *304*, 121379. [CrossRef]
19. Golzari, R.; Zhao, H.; Hall, J.; Bassett, M.; Williams, J.; Pearson, R. Impact of intake port injection of water on boosted downsized gasoline direct injection engine combustion, efficiency and emissions. *Int. J. Engine Res.* **2021**, *22*, 295–315. [CrossRef]
20. Stoumpos, S.; Theotokatos, G. Multiobjective Optimisation of a Marine Dual Fuel Engine Equipped with Exhaust Gas Recirculation and Air Bypass Systems. *Energies* **2020**, *13*, 5021. [CrossRef]
21. Cai, B.; Rui, H.; Zheng, W. Research on Decision Method of EGR Rate of Diesel Engine based on Multi-Objective Optimization. *Intern. Combust. Engine Parts* **2020**, *17*, 1–05.
22. Chongrong, W.U.; Shengli, W.E.I.; Hongrkun, L.U. Research on Multi-Parameter and Multi-Goal Optimization of Diesel Engine Combustion System. *Mach. Des. Manuf.* **2019**, *2*, 13–17.
23. Kamarulzaman, M.K.; Abdullah, A. Multi-Objective Optimization of Diesel Engine Performances and Exhaust Emissions Characteristics of Hermetia Illucens Larvae Oil-Diesel Fuel Blends Using Response Surface Methodology. *Energy Sources Part A Recovery Util. Environ. Eff.* **2020**, *42*, 1–14. [CrossRef]
24. Wang, H.; Gan, H.; Wang, G.; Zhong, G. Emission and Performance Optimization of Marine Four-Stroke Dual-Fuel Engine Based on Response Surface Methodology. *Math. Probl. Eng.* **2020**, *2020*, 1–9. [CrossRef]
25. Sarangi, A.K.; Garner, C.P.; McTaggart-Cowan, G.P.; Davy, M.H.; Hargrave, G.K. The Impact of Intake Pressure On high-EGR Low Temperature Compression Ignition Engine Combustion Using Borescopic Imaging. *Int. J. Engine Res.* **2020**, *22*, 2347–2361. [CrossRef]
26. Teoh, Y.; Huspi, H.; How, H.; Sher, F.; Din, Z.; Le, T.; Nguyen, H. Effect of Intake Air Temperature and Premixed Ratio on Combustion and Exhaust Emissions in a Partial HCCI-DI Diesel Engine. *Sustainability* **2021**, *13*, 8593. [CrossRef]
27. Dai, L.M.; Wang, Q.; Zhang, Z.R.; He, Z.X.; Gao, Z.S. Numerical Simulation of the Combustion and Emissions of HPDI Engine under Different Natural Gas Substitution Rate. *Adv. Mater. Res.* **2014**, *1044–1045*, 362–369. [CrossRef]
28. Jiang, X.; Wei, H.; Zhou, L.; Chen, R. Numerical Study on the Effects of Multiple-Injection Coupled with EGR on Combustion and NOx Emissions in a Marine Diesel Engine. *Energy Procedia* **2019**, *158*, 4429–4434. [CrossRef]
29. Wang, H.; Gan, H.; Theotokatos, G. Parametric investigation of pre-injection on the combustion, knocking and emissions behaviour of a large marine four-stroke dual-fuel engine. *Fuel* **2020**, *281*, 118744. [CrossRef]
30. Two-stroke Project Guides. Available online: https://marine.man-es.com/two-stroke/project-guides (accessed on 23 December 2017).
31. Hongliang, Y.U. *Numerical Research of Combustion Process in Two-Stroke Low-speed LNG/Diesel Marine Dual-Fuel Engine*; Dalian Maritime University: Dalian, China, 2020.
32. List, A. *AVL BOOST Users' Guides*; AVL List GmbH: Graz, Austria, 2016.

33. Woschni, G. *A Universally Applicable Equation for the Instantaneous Heat Transfer Coefficient in the Internal Combustion Engine*; SAE: New York, NY, USA, 2018; pp. 3065–3083.
34. Chuan, R. *Numerical Study on the Performance of Dual-Fuel Marine Engine*; Dalian Maritime University: Dalian, China, 2013.
35. Wang, G. *Simulation on Micro-Pilot Injection Strategy of Marine Medium-Speed Dual Fuel Engine*; Wuhan University of Technology: Wuhan, China, 2017.
36. Liu, H.; Zhang, H.; Wang, H.; Zou, X. Impact of Air Intake Components on NOx Emissions in Low-Speed Marine Diesel Engine. *J. Combust. Sci. Technol.* **2017**, *23*, 313–319.
37. Song, X. Urban Population Growth Model Based on SPSS Regression Analysis. In Proceedings of the 2018 13th International Conference on Computer Science & Education (ICCSE), Colombo, Sri Lanka, 8–11 August 2018; pp. 1–7.
38. Zhang, K.; Li, W.; Han, Y.; Geng, Z.; Chu, C. Production capacity identification and analysis using novel multivariate nonlinear regression: Application to resource optimization of industrial processes. *J. Clean. Prod.* **2021**, *282*, 124469. [CrossRef]
39. Liu, J.; Zhao, H.; Wang, J.; Zhang, N. Optimization of the injection parameters of a diesel/natural gas dual fuel engine with multi-objective evolutionary algorithms. *Appl. Therm. Eng.* **2019**, *150*, 70–79. [CrossRef]
40. Ji, C.; Wang, H.; Shi, C.; Wang, S.; Yang, J. Multi-Objective Optimization of Operating Parameters for a Gasoline Wankel Rotary Engine by Hydrogen Enrichment. *ENERGY Convers. Manag.* **2021**, *229*, 113732. [CrossRef]
41. Feng, Q.; Li, Q.; Quan, W.; Pei, X. Overview of Multi-Objective Particle Swarm Optimization Algorithm. *Chin. J. Eng.* **2021**, *43*, 745–753.
42. Lee, P.P.; Sin, C.N. Improved Efficiency of MOPSO with Adaptive Inertia Weight and Dynamic Search Space. In Proceedings of the GECCO 2018 Genetic and Evolutionary Computation Conference Companion, Kyoto, Japan, 15–19 July 2018; pp. 1910–1913.
43. Tuppadung, Y.; Kurutach, W. Comparing nonlinear inertia weights and constriction factors in particle swarm optimization. *Int. J. Knowledge-based Intell. Eng. Syst.* **2011**, *15*, 65–70. [CrossRef]
44. Van den Bergh, F.; Engelbrecht, A.P. A study of particle swarm optimization particle trajectories. *Inf. Sci.* **2006**, *176*, 937–971. [CrossRef]
45. Huang, Y.; Ma, F. Intelligent regression algorithm study based on performance and NOx emission experimental data of a hydrogen enriched natural gas engine. *Int. J. Hydrogen Energy* **2016**, *41*, 11308–11320. [CrossRef]
46. Wang, H.; Ji, C.; Shi, C.; Ge, Y.; Wang, S.; Yang, J. Development of cyclic variation prediction model of the gasoline and n-butanol rotary engines with hydrogen enrichment. *Fuel* **2021**, *299*, 120891. [CrossRef]
47. Kakati, D.; Roy, S.; Banerjee, R. Development of an artificial neural network based virtual sensing platform for the simultaneous prediction of emission-performance-stability parameters of a diesel engine operating in dual fuel mode with port injected methanol. *Energy Convers. Manag.* **2019**, *184*, 488–509. [CrossRef]
48. Chen, Z.; Li, T.; Wang, B.; Zheng, M. Influence of Intake Pressure on Diesel Micro Ignition Ethanol Engine. *SHIP Eng.* **2017**, *39*, 40–43.
49. Xu, G.; Jia, M.; Li, Y.; Xie, M.; Su, W. Multi-objective optimization of the combustion of a heavy-duty diesel engine with low temperature combustion (LTC) under a wide load range: (II) Detailed parametric, energy, and exergy analysis. *Energy* **2017**, *139*, 247–261. [CrossRef]